RSC Advances

PAPER

View Article Online
View Journal | View Issue



Cite this: *RSC Adv.*, 2026, **16**, 12786

# Stability and hydrogen storage potential of zirconium-based $A_2ZrH_6$ (A = Na, K) hydrides: a DFT and AIMD investigation

Muhammad Kaleem, *[a] Amna Nasir,[a] Zahid Sarfraz,[b] Sanober Kanwal,[c] Asif Nawaz Khan, [d] A. F. Abd El-Rehim[e] and Heba Y. Zahran[e]

Perovskite-based materials offer considerable potential for efficient, stable and environmentally sustainable hydrogen storage technologies. In this work an inclusive density functional theory (DFT) investigation was conducted to evaluate the structural, mechanical, optoelectronic and thermodynamic features of $A_2ZrH_6$ (A = Na, K) perovskite hydrides. Structural analysis reveals the stable cubic $Fm\bar{3}m$ symmetry, supported by favorable tolerance factors (0.92–0.99) and negative formation energies endorsing thermodynamic stability. *Ab initio* molecular dynamics (AIMD) simulations assure thermal stability at 300 K without significant structural distortion. $Na_2ZrH_6$ and $K_2ZrH_6$ exhibit notable hydrogen storage characteristics, achieving 4.22 and 3.45 wt% capacities with desorption temperatures of 441.39 and 258.91 K respectively. Mechanical analysis confirms elastic and Born stability with Poisson's ratios of 0.14 ($Na_2ZrH_6$) and 0.25 ($K_2ZrH_6$) and *B*/*G* ratios of 1.06 and 1.66 indicating brittle behavior. Electronic structure calculations confirm the band gaps of 1.25 and 1.87 eV while optical investigations indicate the suitability of these hydrides for photovoltaic applications. These results highlight $A_2ZrH_6$ (A = Na, K) perovskite hydrides as viable and efficient materials for next-generation hydrogen storage and energy conversion systems.

Received 24th January 2026
Accepted 1st March 2026

DOI: 10.1039/d6ra00660d

rsc.li/rsc-advances



## Introduction

Concerns about the enduring viability of fossil fuel based energy systems have grown as a result of the sharp increase in the world energy demand brought on by industrialization and population expansion.[1–3] Elongated reliance on coal and oil and natural gas has a negative impact on the environment, contributing to climate change and deteriorating air quality.[4] These difficulties have sped up the worldwide hunt for sustainable and clean energy sources that can provide future energy needs with little negative influence on the environment.[5] Due to its high gravimetric energy density, toxic free nature and carbon free combustion products, hydrogen has become a particularly appealing alternative.[6,7] Despite these benefits, the absence of safe, portable and effective hydrogen storage technology continues to be a major barrier to the widespread use of hydrogen energy. It is commonly acknowledged that resolving this issue is one of the most important obstacles to achieving a hydrogen-based energy economy.[8,9]

Solid-state storage of complex metal hydrides has attracted a lot of attention due to its improved safety, high volumetric density and advantageous thermodynamic features as compared to gaseous and liquid hydrogen storage methods. Because of their highly adjustable physicochemical characteristics and structurally flexible frameworks, perovskite and double perovskite hydrides in this family have attracted increased attention.[10,11] The perovskite design enables significant compositional engineering through cation substitution which enables systematic control over hydrogen concentration, lattice stability and electrical performance. Specifically organized octahedral networks made of double perovskite hydrides with the general formula $A_2BB'H_6$ are intriguing options for solid state $H_2$ storage applications because they can tolerate high $H_2$ concentrations without losing structural integrity.[12]

Various double perovskite hydrides have shown aptitude for $H_2$ storage in recent theoretical and experimental studies. Research showed that $XAlH_6$ (X = Ca, Sr, Ba)[13] and $Na_2LiXH_6$ (X = Al, Sc, Ga)[2] and $K_2LiAlH_6$ (ref. 6) demonstrate encouraging $H_2$ storage capacities and structural stability. Other related systems such as $AeSiH_3$ (Ae = Li, Na, K, Mg),[14] $XSrH_3$ (ref. 15) and $A_2BH_6$ type hydrides have also been examined, revealing diverse electronic, mechanical and thermodynamic behaviors. Recent first-

[a]*Material Research Laboratory (MRL), Department of Physics, International Islamic University H-10, Islamabad 44000, Pakistan. E-mail: mkaleemphy@gmail.com*
[b]*Advanced Materials Processing Laboratory, Department of Physics, Air University, Pakistan*
[c]*Research in Modeling and Simulation Group, COMSATS University Islamabad, Pakistan*
[d]*Materials Modeling and Simulation Lab, Department of Physics, University of Science & Technology, Bannu 28100, Khyber Pakhtunkhwa, Pakistan*
[e]*Physics Department, Faculty of Science, King Khalid University, P. O. Box 9004, Abha 61413, Saudi Arabia*

principles studies have further highlighted the potential of double perovskite hydrides for hydrogen storage. For instance Bakar *et al.* investigated double hydrides $Na_2YH_6$ (Y = Ca, Ti) using density functional theory and reported gravimetric $H_2$ storage capacities of 6.17 wt% for $Na_2CaH_6$ and 5.72 wt% for $Na_2TiH_6$.[16] Their electronic structure analysis indicated metallic behavior in $Na_2CaH_6$ whereas $Na_2TiH_6$ exhibited semiconducting character with a band gap of 0.921 eV. Similarly Hakami *et al.* examined the $H_2$ storage, mechanical and optoelectronic properties of $A_2FeH_6$ (A = Be, Mg) double perovskite hydrides reporting gravimetric hydrogen capacities of 7.50 wt% for $Be_2FeH_6$ and 5.43 wt% for $Mg_2FeH_6$ along with wide band gaps of 2.89 and 3.08 eV respectively.[17] In another related study, Ahmed *et al.* explored $X_2FeH_6$ (X = Ca, Sr) hydrides and demonstrated thermodynamic stability and semiconducting behavior with indirect band gaps of 1.67 eV for $Ca_2FeH_6$ and 1.37 eV for $Sr_2FeH_6$ while reporting gravimetric $H_2$ densities of 4.28 wt% and 2.54 wt% respectively.[18]

Despite these advances many reported perovskite hydrides continue to face intrinsic limitations including elevated hydrogen desorption temperatures, sluggish sorption kinetics, limited gravimetric capacity or structural instability under operating conditions.[19] In several instances improvements in $H_2$ capacity have been achieved at the expense of mechanical or dynamical stability underscoring the persistent challenge of balancing hydrogen density with material robustness.[20,21] Motivated by these considerations zirconium based perovskite hydrides represent an attractive yet relatively underexplored class of materials. Zirconium as a tetravalent transition metal provides favorable charge balance and strong metal–hydrogen interactions that can stabilize corner-sharing [$ZrH_6$] octahedra within a perovskite lattice. Alkali metal substitution at the A-site offers an additional degree of freedom to tune lattice dimensions, electronic structure and hydrogen binding strength. In particular the $A_2ZrH_6$ (A = Na, K) family is of significant interest as replacing $Na^+$ with the larger $K^+$ cation is expected to systematically influence structural parameters, thermodynamic stability and hydrogen storage performance. Nevertheless a comprehensive investigation of the structural, mechanical, AIMD stability, $H_2$ storage, optoelectronic and thermodynamic properties of $Na_2ZrH_6$ and $K_2ZrH_6$ remains absent from the literature.

In this work a detailed first-principles investigation of $A_2ZrH_6$ (A = Na, K) perovskite hydrides is performed using density functional theory. The study systematically examines their crystal structure, AIMD stability, elastic and mechanical behavior, electronic band structure and density of states, optical, thermodynamic characteristics and $H_2$ storage performance to establish clear composition-property relationships. By elucidating how alkali metal substitution impacts lattice stability, electrical responsiveness and hydrogen binding behavior this work identifies crucial factors regulating $H_2$ absorption and release in zirconium based perovskite hydrides. The results provide new theoretical insights into this mostly unexplored material class as well as a rational foundation for the design and experimental development of superior solid state $H_2$ storage materials. Future studies will also explore the influence of other alkali metals on these material properties, further broadening the scope of perovskite hydride research.

### Computational methodology

The structural and physical characteristics of the $A_2ZrH_6$ (A = Na, K) perovskite hydrides were investigated using first principles calculations carried out within the context of DFT. The CASTEP code which uses a plane wave pseudopotential method to solve the KohnSham equations was used to carry out the simulations. Vanderbilt ultrasoft pseudopotentials were used to represent electron and ion interactions allowing for an accurate and effective handling of valence electrons. The generalized gradient approximation (GGA) was used to tackle the exchange correlation effects in the Perdew–Burke–Ernzerhof (PBE) formulation.[22–24] The valence electronic configurations explicitly considered in the calculations were Na ($2s^2\ 2p^6\ 3s^1$), K ($3s^2\ 3p^6\ 4s^1$), Zr ($4s^2\ 4p^6\ 4d^2\ 5s^2$) and H ($1s^1$). To guarantee consistent convergence of total energies and stress tensors a plane wave kinetic energy cutoff of 600 eV was used. A Monkhorst–Pack *k*-point mesh of 6 × 6 × 6 was used for Brillouin zone integrations and it was confirmed to yield converged structural and electrical properties.[25] The Broyden–Fletcher–Goldfarb–Shanno (BFGS) minimization approach was used for structural optimizations enabling the simultaneous relaxation of internal atomic coordinates and lattice parameters. The convergence criteria for geometry optimization were set to $2.0 \times 10^{-5}$ eV per atom for total energy 0.05 eV $Å^{-1}$ for maximum force and $2 \times 10^{-3}$ Å for maximum atomic displacement and 0.01 GPa for residual stress.[26] All calculations were conducted under zero-temperature and zero-pressure conditions to determine the ground-state configurations of the investigated hydrides.

To assess thermal stability beyond static calculations *ab initio* molecular dynamics (AIMD) simulations were performed using the pw.x module of Quantum ESPRESSO. The simulations were conducted within the canonical NVT ensemble with temperature control achieved through a Berendsen thermostat set at 300 K. Atomic trajectories were propagated using the velocity-Verlet algorithm with a time step of 0.97 fs over 10 000 steps corresponding to a total simulation time of approximately 9.7 ps. Ultrasoft pseudopotentials consistent with the PBE exchange-correlation functional were employed with plane-wave and charge-density cutoffs of 60 Ry and 400 Ry respectively. The self-consistent field convergence threshold was set to $1.0 \times 10^{-8}$ Ry while total energy and force convergence criteria were fixed at $1.0 \times 10^{-5}$ Ry and $1.0 \times 10^{-4}$ Ry/Bohr respectively.[27]

## Results and discussion

### Structural properties

The structural characteristics and geometric stability of the $A_2ZrH_6$ (A = Na, K) perovskite hydrides were systematically investigated using first-principles DFT calculations. Both compounds crystallize in a highly symmetric cubic structure with space group $Fm\bar{3}m$ (No. 225) preserving the ideal perovskite framework.[28] The atomic arrangements within the cubic unit

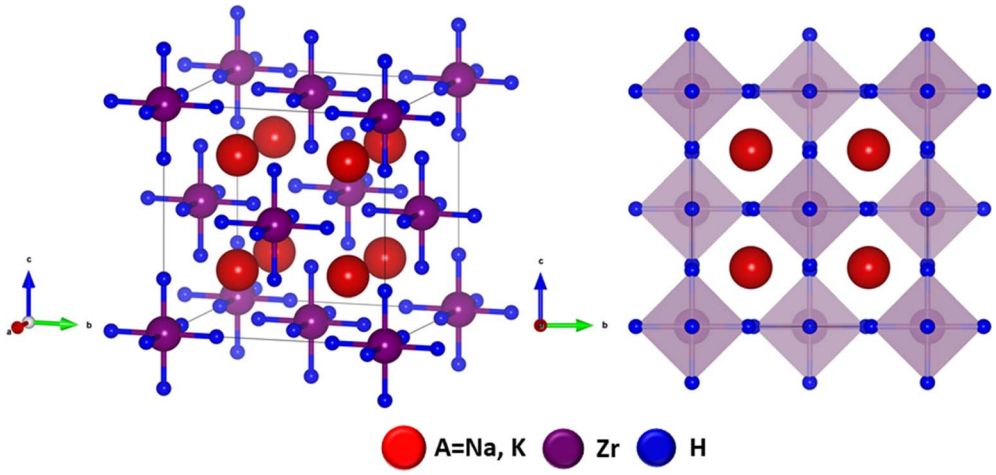


Fig. 1 Optimized crystal structure of $A_2ZrH_6$ (A = Na, K) perovskite hydrides.

cell follow distinct Wyckoff positions in which the A-site cations (Na or K) occupy the 8c sites (0.25, 0.25, 0.25) while Zr atoms are positioned at the 4a sites (0, 0, 0) forming the backbone of the perovskite lattice. The hydrogen atoms be vested at the 24e sites ($x$, 0, 0) where the internal parameter $x = 0.245$ resulting in marginally distorted $ZrH_6$ octahedra as displayed in Fig. 1. This octahedral coordination directly affects hydrogen binding and is essential for maintaining the crystal structure. The optimized lattice constants were found to be 8.31 Å for $Na_2ZrH_6$ and 8.95 Å for $K_2ZrH_6$ with lattice parameters satisfying $a = b = c$ as summarized in Table 1. The observed lattice expansion upon substitution of Na with the larger K cation is further reflected in the computed unit cell volumes which increase from 573.87 $Å^3$ for $Na_2ZrH_6$ to 718.86 $Å^3$ for $K_2ZrH_6$ consistent with the ionic size difference between $Na^+$ and $K^+$.

To further assess geometric stability, the Goldschmidt tolerance factor ($\tau_G$) and octahedral factor ($\mu$) were evaluated using the eqn (1) and (2):[29]

$$\tau_G = \frac{(R_A + R_H)}{\sqrt{2}(R_{Zr} + R_H)} \quad (1)$$

$$\mu = \frac{R_{Zr}}{R_H} \quad (2)$$

where $R_A$, $R_{Zr}$ and $R_H$ denote the ionic radii of the A-site cation (Na or K), Zr and hydrogen respectively. As listed in Table 1 the calculated $\tau_G$ values are 0.92 for $Na_2ZrH_6$ and 0.99 for $K_2ZrH_6$ both lying within the accepted stability range for cubic perovskites. The octahedral factor $\mu$ was found to be 0.47 for both compounds which falls well within the conventional stability window confirming the robustness of the $ZrH_6$ octahedral network.

Moreover the thermodynamic stability of the investigated compounds was further examined through the calculation of the formation energy ($\Delta H_f$) given by eqn (3):[31]

$$\Delta H_f = \frac{E(A_2ZrH_6) - [2E(A) + E(Zr) + 6E(H)]}{n} \quad (3)$$

where $E(A_2ZrH_6)$ is the energy of the compound $E(A)$, $E(Zr)$ and $E(H)$ represent the total energies of the isolated constituent atoms and $n$ is the total number of atoms in the formula unit. The calculated formation energies are −1.33 eV per atom (−57.69 kJ $mol^{-1}$ $H_2$) for $Na_2ZrH_6$ and −0.78 eV per atom (−33.84 kJ $mol^{-1}$ $H_2$) for $K_2ZrH_6$ confirming the exothermic formation and intrinsic thermodynamic stability of both perovskite hydrides. These structural features combined with favorable geometric and thermodynamic stability imply that $A_2ZrH_6$ (A = Na, K) perovskite hydrides provide a robust framework for reversible $H_2$ absorption and release supporting its potential application in solid state $H_2$ storage systems.

## Hydrogen storage

Hydrogen is largely considered as a vital energy vector for achieving a sustainable and low carbon energy future owing to

Table 1 Structural parameters of $A_2ZrH_6$ (A = Na, K) perovskite hydrides

| Parameters | $Na_2ZrH_6$ | $K_2ZrH_6$ | $Sr_2FeH_6$ (ref. 18) | $Ca_2FeH_6$ (ref. 18) | $Sr_2VH_6$ (ref. 30) |
|---|---|---|---|---|---|
| Lattice constant $a = b = c$ (Å) | 8.31 | 8.95 | 5.30 | 4.87 | 7.12 |
| Volume $(Å)^3$ | 573.87 | 718.86 | 148.88 | 115.50 | 59.56 |
| $\tau_G$ | 0.92 | 0.99 | — | — | 0.99 |
| $\mu$ | 0.47 | 0.47 | — | — | 0.47 |
| $\Delta H_f$ | −1.33 | −0.78 | −4.23 | −6.93 | −0.284 |
| $\Delta H_f$(kJ $mol^{-1}$ $H_2$) | −57.69 | −33.84 | — | — | −33.84 |
| $C_{wt\%}$ | 4.22 | 3.45 | 2.54 | 4.28 | 2.60 |
| $T_{des}$ (K) | 441.39 | 258.91 | — | — | 210.7 |

its high gravimetric energy density and environmentally benign utilization. However a significant obstacle to its widespread use is still the absence of safe and portable and effective $H_2$ storage systems. In this sense solid state $H_2$ storage based on complex metal hydrides has garnered a lot of interest since it provides better safety and volumetric efficiency when compared to traditional gaseous and liquid storage techniques. Perovskite derived hydrides particularly $A_2ZrH_6$ (A = Na, K) systems represent a promising class of materials due to their structural robustness and intrinsically high hydrogen content. The gravimetric hydrogen capacity which measures the mass fraction of hydrogen in relation to the total mass of the storage medium is a crucial metric for assessing the efficacy of hydrogen storage. The eqn (4) was used to get the theoretical gravimetric hydrogen capacity:[32]

$$C_{\omega t\%} = \left[\frac{\left(\frac{H}{M}\right)m_H}{m_{Host} + \left(\frac{H}{M}\right)m_H} \times 100\right]\% \quad (4)$$

where $m_{Host}$ and $m_H$ represent the molar masses of the host lattice and hydrogen respectively and $\frac{H}{M}$ denotes the hydrogen to metal ratio. Using this formulation the gravimetric hydrogen capacities of $Na_2ZrH_6$ and $K_2ZrH_6$ were determined to be 4.22 wt% and 3.45 wt% respectively as listed in Table 1. The higher capacity of $Na_2ZrH_6$ originates from the lower atomic mass of sodium which enhances the hydrogen-to-host mass ratio. These values are competitive among complex hydride systems and show a clear possibility for more optimization through compositional adjustment even if they are still below the U.S. DOE 2025 gravimetric target of 5.5 wt%. In addition to storage capacity the hydrogen release behaviour plays a crucial role in practical applications and is commonly assessed through the desorption temperature ($T_{des}$). Desorption temperature can be estimated from thermodynamic considerations based on the Gibbs free energy eqn (5): [33,34]

$$\Delta G = \Delta H - T_{des}\cdot\Delta S \Rightarrow T_{des} = \frac{\Delta H}{\Delta S} \quad (5)$$

where $\Delta H$ and $\Delta S$ denote the enthalpy and entropy changes associated with hydrogen desorption. The computed desorption temperatures for $Na_2ZrH_6$ and $K_2ZrH_6$ using the standard entropy of $H_2$ gas are 441.39 K and 258.91 K respectively (Table 1). While the greater $T_{des}$ of $Na_2ZrH_6$ indicates stronger metal hydrogen contacts and improved thermal stability the somewhat lower desorption temperature of $K_2ZrH_6$ indicates more advantageous hydrogen release under moderate operating conditions. It is important to note that these values are rough estimates based on the standard entropy of gaseous hydrogen. Further experimental and theoretical studies are needed to refine these estimates and provide a more accurate understanding of the hydrogen desorption process. When combined, these findings show that in $A_2ZrH_6$ (A = Na, K) perovskite hydrides gravimetric capacity and $H_2$ release properties are balanced. While $K_2ZrH_6$ shows more accessible desorption behavior $Na_2ZrH_6$ gives a larger $H_2$ storage capacity indicating the potential for compositional engineering to attain optimal $H_2$ storage performance. In comparison to other hydrogen storage materials like $MgH_2$,[35] which has a gravimetric hydrogen capacity of 7.6 wt%, $Na_2ZrH_6$ and $K_2ZrH_6$ show lower capacities. However, $Na_2ZrH_6$ offers a better balance between hydrogen storage capacity and thermal stability, with a desorption temperature ($T_{des}$) of 441.39 K, which is higher than $K_2ZrH_6$ (258.91 K), making it more stable under high-temperature conditions. $K_2ZrH_6$, however, exhibits more accessible hydrogen desorption behavior at lower temperatures, making it more favorable for use under moderate operating conditions.

### *Ab Initio* molecular dynamics (AIMD) calculations

AIMD simulations conducted at room temperature were used to investigate the dynamical and thermal stability of the $A_2ZrH_6$ (A = Na, K) perovskite hydrides as illustrated in Fig. 2(a and b). AIMD simulations provide a realistic assessment of finite temperature behavior by merging first principles electronic structure computations with classical atomic motion and directly evaluating total energy development and thermodynamic stability under thermal agitation.[36] The total energy profile for $Na_2ZrH_6$ is well controlled over the 9.7 ps simulation frame with extremely small amplitude fluctuations around an equilibrium value as seen in Fig. 2(a). Importantly no systematic drift or sudden fluctuation is seen indicating that there is no structural instability during heat stimulation. The temperature evolution continuously varies about the target value of 300 K while remaining within a narrow physically attainable range. This behavior shows that under ambient conditions the $Na_2ZrH_6$ framework does not undergo phase transformation or breakdown and retains its structural integrity. As seen in Fig. 2(b) $K_2ZrH_6$ reacts similarly. A dynamically stable lattice is suggested by the total energy small fluctuations and lack of abrupt discontinuities throughout the trial. With brief fluctuations typical of constant temperature AIMD simulations the associated temperature swings stay centered around room temperature. The mechanical system of $K_2ZrH_6$ and thermal endurance are further supported by the lack of abnormal pressure or temperature variations. These findings which consistently show limited energy routes and steady temperature profiles offer compelling evidence of the thermal and dynamical stability of both $Na_2ZrH_6$ and $K_2ZrH_6$. These perovskite hydrides resilience under practical operating settings is demonstrated by the AIMD simulations lack of structural degradation which further supports their applicability for $H_2$ storage and energy related applications.

### Mechanical properties

Mechanical characteristics exhibit a decisive role in prevailing the elastic response and structural reliability of perovskite hydrides mainly under the cyclic stresses associated with $H_2$ absorption and release.[37] A quantitative evaluation of elastic constants is therefore essential to assess mechanical stability and deformation behavior.[38] In this work the second-order elastic constants ($C_{ij}$) of $A_2ZrH_6$ (A = Na, K) perovskite hydrides were calculated from which key mechanical

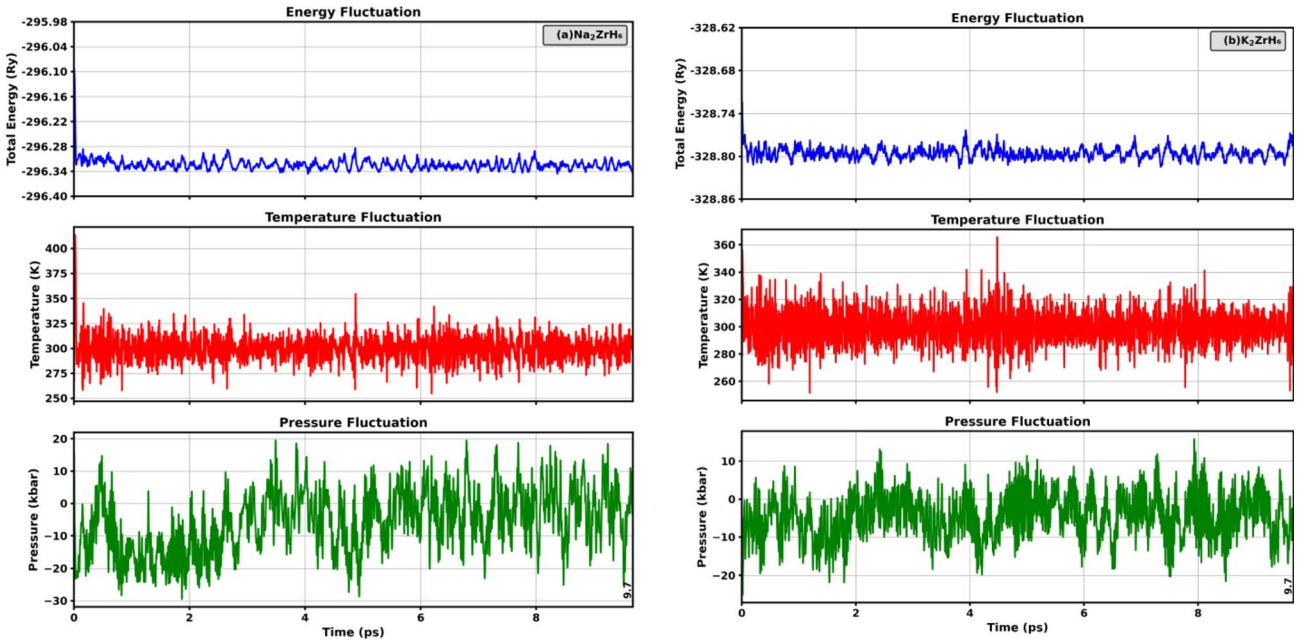


Fig. 2 AIMD total-energy traces *versus* time for (a) $Na_2ZrH_6$ and (b) $K_2ZrH_6$ hydrides.

parameters were derived. The calculated elastic constants and related mechanical properties are summarized in Table 2. Due to the cubic crystal symmetry only three independent elastic constants $C_{11}$, $C_{12}$ and $C_{44}$ are required to describe the elastic behavior of the studied compounds.[39] These constants represent resistance to uniaxial deformation, transverse deformation and shear deformation respectively. The calculated values for both $Na_2ZrH_6$ and $K_2ZrH_6$ satisfy the Born-Huang mechanical stability criteria for cubic crystals: $C_{11} - C_{12} > 0$, $C_{11} + 2C_{12} > 0$, $C_{11} > 0$ and $C_{44} > 0$ confirming that both compounds are mechanically stable under small strains. As shown in Table 2 $Na_2ZrH_6$ exhibits relatively lower elastic stiffness with $C_{11} =$ 19.48 GPa, $C_{12} = 4.41$ GPa and $C_{44} = 9.96$ GPa whereas $K_2ZrH_6$ displays higher longitudinal rigidity with $C_{11} = 54.75$ GPa indicating stronger resistance to uniaxial deformation. The larger $C_{11}$ value of $K_2ZrH_6$ reflects enhanced stiffness along principal crystallographic directions consistent with its expanded lattice framework.

The bulk modulus ($B$) and shear modulus ($G$) were calculated using the Voigt–Reuss–Hill (VRH) approximation in order to assess macroscopic elastic behavior.[40] The shear modulus shows resistance to shape deformation whereas the bulk modulus shows resistance to homogeneous compression. The calculated $B$ values are 9.43 GPa for $Na_2ZrH_6$ and 22.71 GPa for $K_2ZrH_6$ indicating that $K_2ZrH_6$ possesses a higher resistance to volume compression. In a similar vein the shear modulus rises from 8.90 GPa for $Na_2ZrH_6$ to 13.60 GPa for $K_2ZrH_6$ indicating that the K based combination is more stiff. The Young's modulus ($E$) which measures stiffness under uniaxial stress and has values of 20.32 GPa for $Na_2ZrH_6$ and 34.02 GPa for $K_2ZrH_6$ further supports this tendency. These findings show that $Na_2ZrH_6$ is relatively more compliant than $K_2ZrH_6$ which may be helpful for adapting to volume variations during $H_2$ absorption and desorption. However, the comparatively low elastic moduli, particularly for $Na_2ZrH_6$, also indicate mechanical softness, meaning that the material can deform more readily under external or internally generated cycling stresses.

Table 2 Elastic constants calculated for $A_2ZrH_6$ (A = Na, K) perovskite hydrides

| Elastic moduli | $Na_2ZrH_6$ | $K_2ZrH_6$ | $Sr_2FeH_6$ (ref. 18) | $Ca_2FeH_6$ (ref. 18) | $Sr_2VH_6$ (ref. 30) |
|---|---|---|---|---|---|
| $C_{11}$ | 19.48 | 54.75 | 95.38 | 117.19 | 67.75 |
| $C_{12}$ | 4.41 | 6.69 | 17.32 | 26.99 | 12.32 |
| $C_{44}$ | 9.96 | 9.11 | 30.14 | 38.78 | 21.56 |
| Born's stability | Stable | Stable | Stable | Stable | Stable |
| $B$ (GPa) | 9.43 | 22.71 | 43.34 | 57.06 | 30.79 |
| $G$ (GPa) | 8.90 | 13.60 | 33.42 | 41.19 | 23.84 |
| $E$ (GPa) | 20.32 | 34.02 | 79.75 | 99.60 | 56.86 |
| $B/G$ | 1.06 | 1.66 | 1.29 | 1.38 | 1.23 |
| $\nu$ | 0.14 | 0.25 | — | — | 0.19 |
| $A^U$ | 0.09 | 1.22 | 0.77 | 0.86 | 0.778 |
| $C_p$ | −5.55 | −2.42 | — | — | −9.24 |

Additionally the ductile or brittle nature of the materials was assessed using Pugh ratio ($B/G$) and Poisson's ratio ($\nu$). According to criteria materials with $B/G > 1.75$ and $\nu > 0.26$ exhibit ductile nature.[41] The computed $B/G$ ratios of 1.06 ($Na_2ZrH_6$) and 1.66 ($K_2ZrH_6$) along with Poisson's ratios of 0.14 and 0.25 respectively indicate that both compounds exhibit a predominantly brittle mechanical character with $K_2ZrH_6$ lying close to the brittle or ductile transition. Elastic anisotropy was quantified using the universal anisotropy index ($A^U$). The low value of $A^U = 0.09$ for $Na_2ZrH_6$ suggests near isotropic elastic behavior whereas the higher value of $A^U = 1.22$ for $K_2ZrH_6$ indicates pronounced elastic anisotropy and direction dependent deformation characteristics. Additional insight into bonding nature was obtained from the Cauchy pressure ($C_p = C_{12} - C_{44}$) which yields negative values of −5.55 GPa for $Na_2ZrH_6$ and −2.42 GPa for $K_2ZrH_6$. The unfavorable brittle mechanical behavior in hydride systems is frequently linked to a directed and covalent bonding character, as suggested by Cauchy pressures. From a practical perspective, the combination of low stiffness and brittleness presents both advantages and challenges for hydrogen cycling. While the low moduli can help absorb volumetric strain during repeated $H_2$ absorption and desorption, reducing stress buildup, the brittle nature may lead to crack formation, particle fragmentation, and loss of structural integrity over time, especially under uneven stresses or microstructural defects. Thus, although the current elastic analysis confirms stability under small strains, a full assessment of cycling durability would require further studies focused on fracture behavior and microstructural impacts, which are beyond the scope of this work. Overall, the calculated elastic parameters indicate that $A_2ZrH_6$ (A = Na, K) perovskite hydrides are mechanically stable under small strains, exhibit moderate stiffness, and predominantly brittle behavior, which should be considered when interpreting their ability to withstand structural stresses during repeated hydrogen absorption and release cycles, as shown in the elastic constants and derived mechanical parameters in Table 2.

## Electronic properties

Electronic characteristics play a central role in governing hydrogen adsorption–desorption kinetics, charge redistribution and chemical stability in complex hydrides. In perovskite hydrides the magnitude and nature of the electronic band gap together with the distribution of electronic states near the Fermi level directly influence hydrogen binding strength and diffusion pathways.[42,43] To elucidate these effects the electronic band structures and DOS of $A_2ZrH_6$ (A = Na, K) were systematically analyzed using first principles calculations. The calculated electronic band structures of $Na_2ZrH_6$ and $K_2ZrH_6$ along the high symmetry directions X–R–M–Γ–R are presented in Fig. 3(a and b) with the Fermi level ($E_F$) aligned at 0 eV. A substantial separation between the valence and conduction bands characterizes these materials semiconducting nature. $Na_2ZrH_6$ has an indirect band gap of about 1.25 eV because the valence band maximum and conduction band minimum occur at distinct symmetry sites. This restrained band gap validates

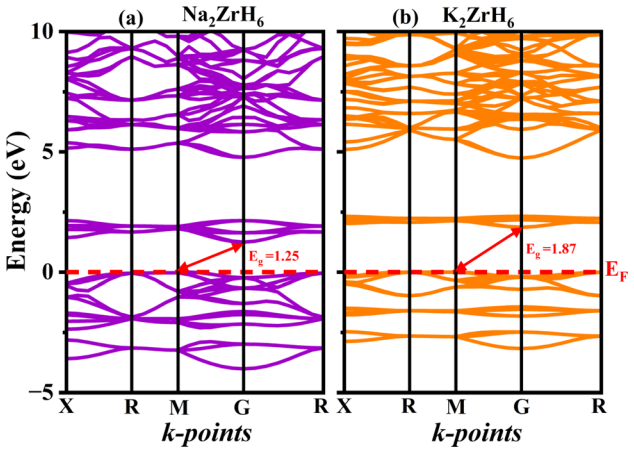


Fig. 3 Computed band structures of (a) $Na_2ZrH_6$ and (b) $K_2ZrH_6$ perovskite hydrides.

that there is enough electronic insulation to prevent undesired electronic leakage while permitting charge redistribution during $H_2$ absorption and release. $K_2ZrH_6$ on the other hand exhibits a broader indirect band gap of roughly 1.87 eV which is a result of the greater $K^+$ ionic radius expanding the lattice and decreasing orbital overlap inside the Zr–H framework. During repeated hydrogen cycling, the increasing band gap suggests improved electronic stability which may be advantageous for preserving structural integrity.[44] The fact that both hydrides are semiconducting implies that electron transport is regulated rather than metallic. Improved reversibility and fewer parasitic processes in $H_2$ storage materials are often associated with this feature.

The total density of states (TDOS) displayed in Fig. 4(a and b) provides further information on the electrical response. The TDOS shows a significant depletion of states at the Fermi level in both $Na_2ZrH_6$ and $K_2ZrH_6$ supporting the band structure findings and verifying their semiconducting nature. The lack of finite DOS at $E_F$ suggests electronic passivation which reduces electronic contributions to structural degradation under operating conditions and aids in stabilizing the $H_2$ rich lattice. The TDOS peaks pronounced asymmetry near the Fermi level indicates that the effective masses of electrons and holes are different. Reaction kinetics may be impacted by this asymmetry potential to affect charge redistribution during hydrogen uptake and release.

The partial density of states (PDOS) for $Na_2ZrH_6$ and $K_2ZrH_6$ displayed in Fig. 4(c and d) reveals the orbital origins of the electronic bands. In both compounds the valence band region below $E_F$ is dominated by H-s states with appreciable hybridization from Zr-d and alkali metal s/p orbitals. This hybridization reflects mixed ionic-covalent bonding within the $ZrH_6$ octahedra which is essential for reversible hydrogen binding. Above the Fermi level the conduction bands are primarily governed by Zr-4d states with secondary contributions from Na-3p or K-4p orbitals. The stronger Zr-d character in the conduction manifold indicates that electronic excitation and charge transfer during hydrogen release are mainly mediated through the

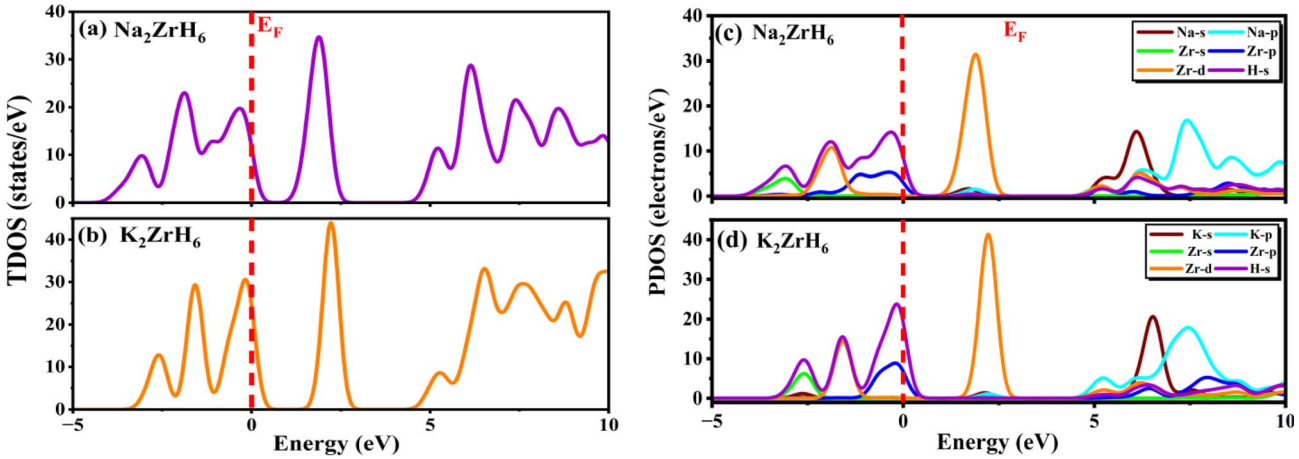


Fig. 4 (a–d): TDOS and PDOS of $A_2ZrH_6$ (A = Na, K) perovskite hydrides.

Zr–H network. Compared to $Na_2ZrH_6$, $K_2ZrH_6$ shows a slightly reduced overlap between Zr-d and H-s states near the band edges consistent with its larger band gap and expanded lattice.

Both $Na_2ZrH_6$ and $K_2ZrH_6$ are indirect gap semiconductors with band gaps falling in a region that combines electrical stability and bonding flexibility according to the combined band structure and DOS investigations. The $ZrH_6$ octahedra play a crucial role in regulating $H_2$ retention and release as evidenced by the preponderance of H(s) states in the valence band and Zr(d) states in the conduction band. While retaining enough electronic flexibility to enable reversible sorption processes these electronic characteristics promote stable $H_2$ accommodation.

## Optical properties

The optical response provides direct insight into photon matter interaction in semiconducting hydride perovskites and is closely linked to interband transitions across the band gap. In $H_2$ storage hydrides such photoexcited carrier generation and associated dielectric screening might promote charge redistribution and localized heating supporting surface reaction steps and influencing absorption desorption rates.[45] This connection between optical properties and hydrogen storage/release performance is important, as the photo-induced carrier excitation can enhance charge redistribution, which supports the surface reaction steps crucial for hydrogen release.

To clarify these effects the frequency dependent optical properties of $A_2ZrH_6$ (A = Na, K) were evaluated. The computed dielectric function and the derived optical spectra are presented in Fig. 5(a–f). The optical response is designated by the complex dielectric function $\varepsilon(\omega) = \varepsilon_1(\omega) + \varepsilon_2(\omega)$ where $\varepsilon_1(\omega)$ reflects dispersion (polarization) and $\varepsilon_2(\omega)$ represents absorption due to interband transitions.[46] As shown in Fig. 5(a) both compounds exhibit finite static dielectric constants indicating measurable low-energy electronic polarizability. $Na_2ZrH_6$ displays a higher static dielectric constant of approximately $\varepsilon_1(0)$ 4.6 whereas $K_2ZrH_6$ shows a lower value of about $\varepsilon_1(0)$ 3.3 reflecting stronger dielectric screening and enhanced polarization in the Na-based hydride. With increasing photon energy $\varepsilon_1(\omega)$ decreases gradually and exhibits pronounced dispersion features before crossing zero in the 3.5–4.0 eV range for $Na_2ZrH_6$ and slightly above 4.2 eV for $K_2ZrH_6$ indicating the effective plasma frequency and the transition from reflective to transparent behavior. At higher energies $\varepsilon_1(\omega)$ attains weakly negative values followed by stabilization, a response characteristic of semiconductors governed by interband transitions rather than free-carrier (Drude) contributions.

The imaginary part $\varepsilon_2(\omega)$ also shown in Fig. 5(a) exhibits an earlier onset for $Na_2ZrH_6$ at 1.3 eV consistent with its smaller electronic band gap ($E_g = 1.25$ eV) while $K_2ZrH_6$ shows a delayed onset near 1.9 eV in agreement with its wider gap ($E_g = 1.87$ eV). For $Na_2ZrH_6$ $\varepsilon_2(\omega)$ displays prominent absorption peaks centered around 2.6 eV and 5.8 eV with a maximum intensity approaching $\varepsilon_2$ of 5.0 whereas $K_2ZrH_6$ exhibits comparatively weaker peaks near 3.0 eV and 6.2 eV reaching a maximum of $\varepsilon_2$ 4.0. These dominant spectral features originate from interband transitions between H-derived valence states and Zr-d dominated conduction states as corroborated by the DOS analysis.[47] The stronger $\varepsilon_2(\omega)$ response of $Na_2ZrH_6$ indicates higher transition probability and enhanced photon-induced carrier excitation which can facilitate charge redistribution and support hydrogen desorption processes under optical or thermal stimulation. This enhanced carrier excitation directly influences hydrogen release, with $Na_2ZrH_6$ showing a stronger capability to drive the desorption process through photon stimulation. The absorption coefficient is obtained from the extinction coefficient $k(\omega)$ through equation $\alpha(\omega) = \frac{2\omega}{c}k\omega$.[48] In Fig. 5(b) both materials show negligible absorption at very low energies followed by a clear rise after the band-edge region. $Na_2ZrH_6$ exhibits the stronger absorption across the spectrum, including a low-energy feature around 2–3 eV (peak $\alpha \sim 3.0 \times 10^4$ cm$^{-1}$) and a dominant high-energy band in the near-UV where the absorption reaches $\alpha \approx 1.7 \times 10^5$ cm$^{-1}$ (around 7–8 eV). In parallel, $K_2ZrH_6$ peaks at $\alpha \approx 1.2$–$1.3 \times 10^5$ cm$^{-1}$ in the same region. The stronger $\alpha(\omega)$ for $Na_2ZrH_6$ indicates more intense photon–electron coupling which can support photo-

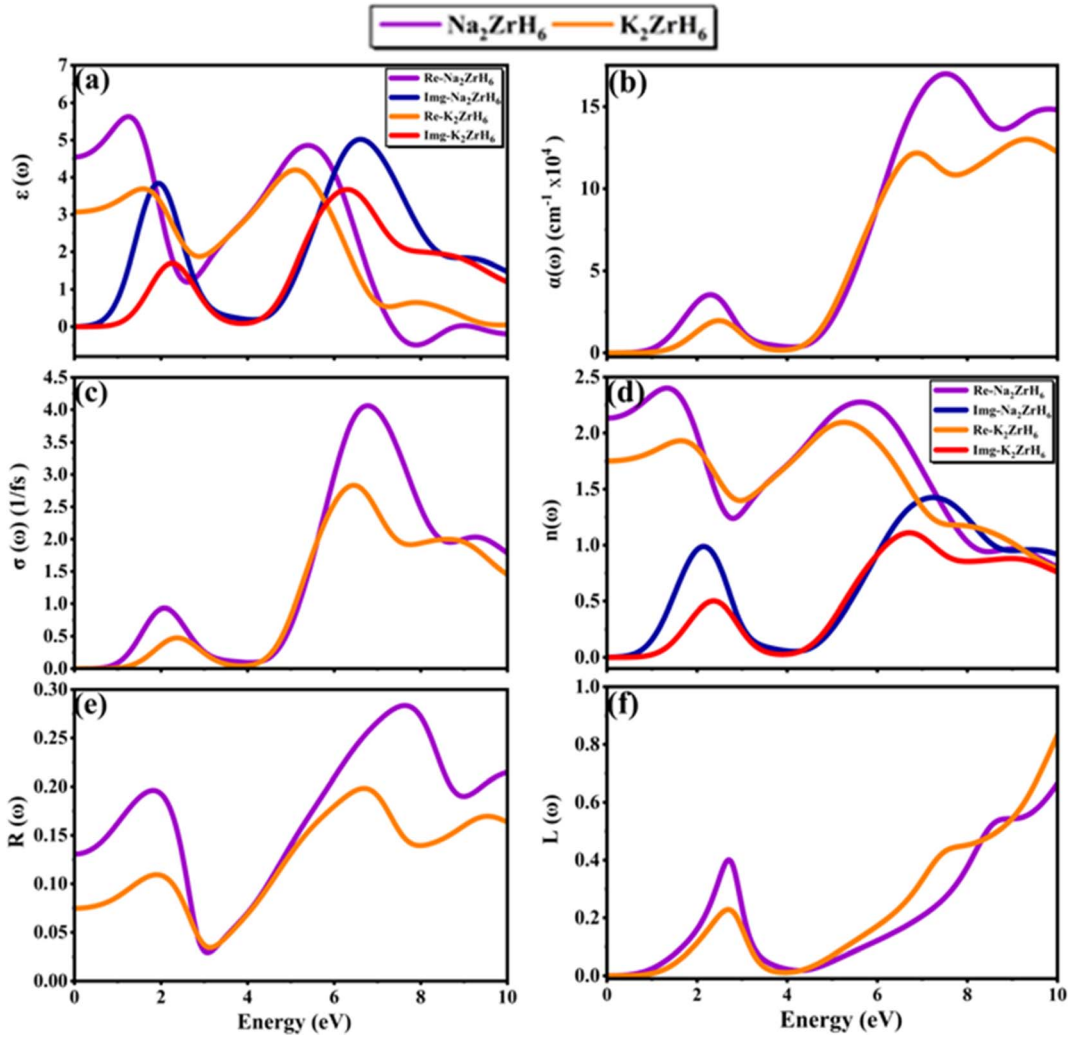


Fig. 5 (a–f): The computed graphs of optical parameters (a) real and imaginary $\varepsilon(\omega)$ (b) absorption spectrum $\alpha(\omega)$ (c) optical conductivity $\sigma(\omega)$ (d) refractive index $n(\omega)$ and extinction coefficient $k(\omega)$ (e) reflectivity $R(\omega)$ and (f) loss function $L(\omega)$ for $A_2ZrH_6$ (A = Na, K) perovskite hydrides.

assisted carrier excitation and localized thermal effects relevant to hydrogen release. This stronger coupling can directly facilitate more efficient photon-driven hydrogen desorption.

Optical conductivity $\sigma(\omega)$ describes the frequency-dependent response of charge carriers under an external electromagnetic field and directly reflects photon-induced electronic transitions that govern photo assisted charge transport and hydrogen desorption dynamics. The optical conductivity can be expressed as $\sigma = \frac{\alpha nc}{4\pi}$.[49] In Fig. 5(c) both compounds show conductivity features that track the absorption bands. $Na_2ZrH_6$ reaches a higher peak optical conductivity (4.0 in the plotted units) near 6–7 eV whereas $K_2ZrH_6$ peaks at a lower magnitude (2.8) in the same region confirming stronger photoinduced carrier activity in the Na-based hydride.

The refractive index and extinction coefficient provide further insight into light propagation and attenuation inside the material and are particularly relevant for assessing light-matter interaction strength in semiconducting hydrides. As evident from Fig. 5(d) both $Na_2ZrH_6$ and $K_2ZrH_6$ exhibit relatively high refractive indices in the low-energy region, consistent with their semiconducting nature and finite band gaps. $Na_2ZrH_6$ shows a higher static refractive index, with $n(0) \approx 2.1$–$2.3$ compared to $n(0)$ 1.7–1.9 for $K_2ZrH_6$ indicating stronger electronic polarization and enhanced photon coupling at low photon energies. The refractive index $n(\omega)$ and extinction coefficient $k(\omega)$ are consequent from the real and imaginary parts of the dielectric function using eqn (6).[50]

$$n(\omega) = \frac{1}{\sqrt{2}}\left(\sqrt{{\varepsilon_1}^2\omega + {\varepsilon_2}^2\omega} + \varepsilon_1(\omega)\right)^{\frac{1}{2}} \cdot k(\omega)$$
$$= \frac{1}{\sqrt{2}}\left(\sqrt{{\varepsilon_1}^2\omega + {\varepsilon_2}^2\omega} - \varepsilon_1(\omega)\right)^{\frac{1}{2}}; \quad (6)$$

As shown in Fig. 5(d) the refractive index of both compounds gradually decreases with increasing photon energy and approaches unity beyond 7 eV reflecting reduced light-matter interaction in the high energy ultraviolet region. The consistently larger $n(\omega)$ values for $Na_2ZrH_6$ across the visible range indicate stronger dispersion and improved optical confinement

which can assist photon-assisted charge excitation relevant for hydrogen release. Significant absorption features in the visible range are revealed by the extinction coefficient spectra which are also shown in Fig. 5(d). While $K_2ZrH_6$ displays a relatively weaker peak with $k_{max}$ 0.5 and $Na_2ZrH_6$ displays a prominent extinction peak about 2–3 eV with $k_{max}$ 1.0. Both materials exhibit wider extinction bands that extend into the UV region at higher energies which are linked to interband electronic transitions involving Zr-d and H-s states. Stronger electromagnetic wave attenuation and improved absorption efficiency which might encourage localized heating and speed up hydrogen desorption processes are confirmed by the greater extinction coefficient of $Na_2ZrH_6$.

Reflectivity $R(\omega)$ quantifies the fraction of incident electromagnetic radiation reflected from the material surface and provides insight into surface optical response absorption efficiency and photon matter coupling which are relevant for light assisted hydrogen absorption and desorption processes can be calculated using eqn (7).[51]

$$R(\omega) = \left|\frac{\sqrt{\varepsilon(\omega)} - 1}{\sqrt{\varepsilon(\omega)} + 1}\right|^2 \quad (7)$$

As shown in Fig. 5(e) both materials exhibit low-to-moderate reflectance with a pronounced minimum around 3 eV (down to 0.03–0.05) coincident with strong absorption. At higher energies $Na_2ZrH_6$ attains a larger reflectivity maximum of 0.28 near 7–8 eV while $K_2ZrH_6$ peaks at 0.20 in a similar range indicating a comparatively stronger reflective response of the Na compound in the near-UV. The energy-loss function provides insight into collective electronic excitations and plasmonic behavior describing the energy dissipated by fast electrons traversing the material and serving as a sensitive indicator of dielectric screening and electronic stability and calculated by eqn (8).[52]

$$L(\omega) = \frac{\varepsilon_2(\omega)}{\left(\varepsilon_1(\omega)^2 + \varepsilon_2(\omega)^2\right)} \quad (8)$$

In Fig. 5(f) both compounds show a clear low-energy loss peak near ≈2–3 eV ($Na_2ZrH_6$: $L_{max}$ 0.40 and $K_2ZrH_6$: $L_{max}$ 0.25) followed by a gradual increase at higher energies. Toward 10 eV $K_2ZrH_6$ rises more strongly (approaching 0.85) than $Na_2ZrH_6$ (0.65) suggesting comparatively higher high energy loss in the K-based hydride.

Overall both $A_2ZrH_6$ (A = Na, K) compounds exhibit semiconducting optical responses with absorption onsets governed by their band gaps and dominant interband activity in the visible-to-UV range. Across Fig. 5(a–f) $Na_2ZrH_6$ consistently shows stronger dielectric screening, higher absorption and larger optical conductivity indicating more efficient photon-driven electronic excitation which can be beneficial for photo-assisted processes and thermally supported hydrogen cycling.

## Thermodynamic properties

Thermodynamic properties play a central role in determining the feasibility and kinetic performance of hydrogen storage materials. Parameters such as sound velocities, Debye temperature ($\theta_D$) and melting temperature ($T_m$) provide indirect yet reliable insight into lattice stiffness, bond strength, phonon transport and thermal robustness. In $H_2$ storage systems these features directly influence hydrogen diffusion kinetics and absorption desorption reversibility and resistance to structural degradation during repeated thermal cycling. In this context elastic constants serve as a fundamental basis for evaluating the thermodynamic stability of $A_2ZrH_6$ (A = Na, K) perovskite hydrides. The longitudinal ($v_l$) and transverse ($v_t$) sound velocities were derived from the bulk modulus ($B$) or shear modulus ($G$) and were used to calculate the average sound velocity ($v_m$). The Debye temperature and melting temperature were subsequently estimated using definite eqn (9)–(11):[53,54]

$$v_l = \sqrt{\frac{3B + 2G}{3\rho}};\quad v_t = \sqrt{\frac{G}{\rho}} \rightarrow v_m = \left[\frac{1}{3}\left(\frac{2}{{v_t}^3} + \frac{1}{{v_l}^3}\right)\right]^{\frac{-1}{3}} \quad (9)$$

$$\theta_D = \frac{h}{k_B}\left[\frac{3nN_a\rho}{4\pi M}\right]^{\frac{1}{3}} \times v_m \quad (10)$$

$$T_m = [553 + 5.911(C_{11})] \pm 300 \quad (11)$$

where $h$ is Planck's constant, $k_B$ represents Boltzmann's constant and $n$ is the number of atoms per formula unit, $N_a$ is Avogadro's number, $M$ is the molecular mass and $C_{11}$ is the elastic constant. The calculated thermodynamic parameters for $Na_2ZrH_6$ and $K_2ZrH_6$ are summarized in Table 3. For $Na_2ZrH_6$ the longitudinal and transverse sound velocities are 3.04 km $s^{-1}$ and 2.32 km $s^{-1}$ respectively resulting in an average sound velocity of 2.48 km $s^{-1}$. These values result in a Debye temperature of 293 K which indicates phonon activity and moderate lattice stiffness. Under moderate temperature circumstances the corresponding melting temperature of 668 K indicates adequate thermal stability for $H_2$ storage operations. In parallel $K_2ZrH_6$ exhibits enhanced elastic wave propagation with $v_l$ = 4.43 km $s^{-1}$ and $v_t$ = 2.90 km $s^{-1}$ and $v_m$ = 3.18 km $s^{-1}$. Stronger interatomic bonds and less lattice anharmonicity are reflected in the higher Debye temperature of 348 K that results from the higher sound velocities. Furthermore greater thermal robustness and resistance to structural weakening at high temperatures are confirmed by the enhanced melting temperature of 877 K. Overall the thermodynamic indicators listed in Table 3 demonstrate that both $A_2ZrH_6$ (A = Na, K) perovskite hydrides possess sufficient lattice stability to support reversible hydrogen absorption and release. The maximum $\theta_D$ and $T_m$ values of $K_2ZrH_6$ suggest improved resistance to thermal degradation

Table 3 Thermal parameters calculated for $A_2ZrH_6$ (A = Na, K) perovskite hydrides

| Compounds | $v_l$ (km $s^{-1}$) | $v_t$ (km $s^{-1}$) | $v_m$ (km $s^{-1}$) | $\theta_D$ (K) | $T_m$ (K) |
|---|---|---|---|---|---|
| $Na_2ZrH_6$ | 3.04 | 2.32 | 2.48 | 293 | 668 |
| $K_2ZrH_6$ | 4.43 | 2.90 | 3.18 | 348 | 877 |

and more stable $H_2$ storage kinetics while $Na_2ZrH_6$ offers a balance between lattice flexibility and thermal integrity encouraging for efficient $H_2$ diffusion.

## Conclusion

This work presents a comprehensive first principles investigation of $A_2ZrH_6$ (A = Na, K) double perovskite hydrides employing DFT calculations within the CASTEP framework to evaluate their potential for $H_2$ storage and clean energy applications. The structural stability of both compounds is confirmed by their cubic $Fm\bar{3}m$ symmetry crystallization and their thermodynamic stability is further supported by negative formation enthalpies. By proving that both compounds retain structural stability at 300 K AIMD provides more evidence for thermal stability. According to mechanical analysis both compounds have a mechanical character that is primarily brittle and satisfy the Born stability requirements. The optical response shows high static dielectric constants and significant absorption in the ultraviolet area while the electronic study shows semiconducting band gaps of 1.25 and 1.87 eV for $Na_2ZrH_6$ and $K_2ZrH_6$ respectively. The calculated gravimetric $H_2$ storage capacities of 4.22 wt% for $Na_2ZrH_6$ and 3.45 wt% for $K_2ZrH_6$ approach the U.S. DOE targets while their corresponding desorption temperatures of 441.39 K and 258.91 K respectively underscore their promising potential for next-generation solid state $H_2$ storage technologies. These results suggest that $A_2ZrH_6$ hydrides offer a promising combination of high $H_2$ storage capacity, thermodynamic viability and structural integrity making them great candidates for future $H_2$ storage and energy delivery systems.

## Conflicts of interest

All authors declare that they have no conflicts of interest.

## Data availability

Data relevant to this study is available upon request.

## Acknowledgements

The authors extend their appreciation to the Deanship of Research and Graduate Studies at King Khalid University for funding this work through Large Research Project under grant number RGP2/140/46.

## References

1 A. Züttel, Hydrogen storage methods, *Naturwissenschaften*, 2004, **91**(4), 157–172.
2 A. Ayyaz, Q. Mahmood, N. D. Alkhaldi, G. Murtaza, A. Usman, M. A. Ullah and H. Albalawi, Exploring hydrogen storage potential, thermodynamic, and optoelectronic characteristics of novel double perovskite hydrides Na2LiXH6 (X= Al, Sc, and Ga): DFT analysis, *J. Energy Storage*, 2025, **122**, 116650.
3 A. Gencer, G. Surucu and S. Al, MgTiO3Hx and CaTiO3Hx perovskite compounds for hydrogen storage applications, *Int. J. Hydrogen Energy*, 2019, **44**(23), 11930–11938.
4 C. Zou, Q. Zhao, G. Zhang and B. Xiong, Energy revolution: From a fossil energy era to a new energy era, *Nat. Gas Ind. B*, 2016, **3**(1), 1–11.
5 M. A. Ullah, M. Kaleem, A. Nasir, Z. Sarfraz, M. M. A. Iqbal, M. Rizwan, K. N. Riaz and M. Tanzeel, An approach towards next-generation hydrogen storage: a DFT study on A 2 LiTiH 6 (A= K, Ca) perovskite hydrides, *RSC Adv.*, 2025, **15**(46), 38714–38728.
6 M. Baaddi, R. Chami, O. Baalla, S. E. Quaoubi, A. Saadi, L. E. H. Omari and M. Chafi, The effect of strain on hydrogen storage characteristics in K 2 NaAlH 6 double perovskite hydride through first principle method, *Environ. Sci. Pollut. Res.*, 2024, **31**(53), 62056–62064.
7 M. Tahir, M. Usman, J. U. Rehman and M. B. Tahir, A first-principles study to investigate the physical properties of Sn-based hydride perovskites XSnH3 (X= K, Li) for hydrogen storage application, *Int. J. Hydrogen Energy*, 2024, **50**, 845–853.
8 S. Niaz, T. Manzoor and A. H. Pandith, Hydrogen storage: Materials, methods and perspectives, *Renew. Sustain. Energy Rev.*, 2015, **50**, 457–469.
9 B. Chen, L. J. Conway, W. Sun, X. Kuang, C. Lu and A. Hermann, Phase stability and superconductivity of lead hydrides at high pressure, *Phys. Rev. B*, 2021, **103**(3), 035131.
10 G. Surucu, A. Gencer, A. Candan, H. H. Gullu and M. Isik, CaXH3 (X= Mn, Fe, Co) perovskite-type hydrides for hydrogen storage applications, *Int. J. Energy Res.*, 2020, **44**(3), 2345–2354.
11 R. Song, Y. Chen, S. Chen, N. Xu and W. Zhang, First-principles to explore the hydrogen storage properties of XPtH3 (X= Li, Na, K, Rb) perovskite type hydrides, *Int. J. Hydrogen Energy*, 2024, **57**, 949–957.
12 A. Ayyaz, M. A. Ullah, M. Zaman, N. D. Alkhaldi, Q. Mahmood, I. Boukhris, M. Al-Buriahi and M. mana Al-Anazy, Investigation of hydrogen storage and energy harvesting potential of double perovskite hydrides A2LiCuH6 (A= Be/Mg/Ca/Sr): A DFT approach, *Int. J. Hydrogen Energy*, 2025, **102**, 1329–1339.
13 M. Umer, G. Murtaza, N. Ahmad, A. Ayyaz, H. H. Raza, A. Usman, A. Liaqat and S. Manoharadas, First principles investigation of structural, mechanical, thermodynamic, and electronic properties of Al-based perovskites XAlH3 (X= K, Rb, Cs) for hydrogen storage, *Int. J. Hydrogen Energy*, 2024, **61**, 820–830.
14 A. Mera and M. A. Rehman, First-principles investigation for the hydrogen storage properties of AeSiH3 (Ae= Li, K, Na, Mg) perovskite-type hydrides, *Int. J. Hydrogen Energy*, 2024, **50**, 1435–1447.
15 H. H. Raza, G. Murtaza, N. Muhammad and S. M. Ramay, First-principle investigation of XSrH3 (X= K and Rb) perovskite-type hydrides for hydrogen storage, *Int. J. Quantum Chem.*, 2020, **120**(24), e26419.
16 A. Bakar, M. Ahmed, Q. Xia, J. Yang, A. Afaq and Y. Yang, Conceptual design and stand-alone multiscale simulation

for hydrogen storage energy: A rigorous way forward for double hydride perovskites Na2YH6 (Y= Ca, Ti), *Int. J. Hydrogen Energy*, 2026, **197**, 152679.

17 O. Hakami and H. J. Alathlawi, Study of mechanical, optoelectronic, and thermoelectric characteristics of Be/Mg ions Based double perovskites $A_2FeH_6$ (A= Be, Mg) for hydrogen storage applications, *Int. J. Hydrogen Energy*, 2024, **83**, 307–316.

18 B. Ahmed, M. B. Tahir, A. Ali and M. Sagir, DFT insights on structural, electronic, optical and mechanical properties of double perovskites X2FeH6 (X= Ca and Sr) for hydrogen-storage applications, *Int. J. Hydrogen Energy*, 2024, **50**, 316–323.

19 S. Al, M. Yortanlı and E. Mete, Lithium metal hydrides (Li2CaH4 and Li2SrH4) for hydrogen storage; mechanical, electronic and optical properties, *Int. J. Hydrogen Energy*, 2020, **45**(38), 18782–18788.

20 A. Hosen, A. Sadeghi, H. A. Abdulhussein, E. Nemati-Kande, A. N. Khan, H. Bekkali, A. Akremi and I. Boukhris, First-principles insights into NaScQH6 (Q= Fe, Ru, Os): Promising high-density hydrogen storage materials, *Int. J. Hydrogen Energy*, 2025, **177**, 151392.

21 M. mana Al-Anazy, G. M. Mustafa, O. Zayed, B. Younas, T. M. Al-Daraghmeh, N. D. Alkhaldi, A. S. Alofi, A. K. Alqorashi and Q. Mahmood, Study of alkaline metals hydrides RbXH3 (X= Mg/Ca/Sr/Ba) for green energy and hydrogen storage applications, *Int. J. Hydrogen Energy*, 2024, **78**, 927–937.

22 W. Khan, Computational screening of BeXH3 (X: Al, Ga, and In) for optoelectronics and hydrogen storage applications, *Mater. Sci. Semicond. Process.*, 2024, **174**, 108221.

23 M. Z. Abbasi, A. U. Rehman, M. Sheraz, W. U. K. Tareen, M. Kaleem, S. T. Jan, H. Ali and T. C. Chuah, Enhancing the performance of lead-free CsInCl3 perovskite solar cells with Ag and Au plasmonic nanoparticles: A DFT and SCAPS-1D analysis, *Results Eng.*, 2025, 105043.

24 M. Ali, Z. Bibi, S. Kanwal, T. Fatima, M. Raheel, A. F. Khan and M. Kaleem, A comprehensive investigation of structural, mechanical and optoelectronics attributes of M2AsC (M= Zr, Hf, Ta, W) MAX phase carbides: A DFT investigation, *J. Mol. Graph. Model.*, 2025, 109102.

25 R. J. Meier, On the effectiveness of ultra-soft pseudopotentials in plane-wave based molecular electronic structure calculations, *J. Mol. Struct.*, 1999, **467**(1), 79–83.

26 A. Hussain, N. Jabeen, A. Yaqoob, A. Smerat, M. A. Qaiser and N. A. Aldawsari, Hydrogen Storage Capacity and Optoelectronic Response of Mechanically and Thermally Stable Lithium-Based Tetrahydrates (LiXH4, X= B, Al, Mn), a DFT Approach, *Crystals*, 2025, **15**(11), 990.

27 A. N. Khan, M. Kaleem, N. U. Khan, A. Nasir, A. Khan and M. Z. Abbasi, Multi-functional DFT and SCAPS-1D analysis of lead-free Z2MgGeI6 (Z= Na, K) double perovskites for optoelectronic, photo-catalytic, and photovoltaic applications, *Sol. Energy Mater. Sol. Cells*, 2026, **294**, 113922.

28 Z. Abbas, A. Alqahtani, K. Bibi, A. Parveen, Z. Bayhan, A. El-Rayyes and M. T. Khan, First-principles study of structural, electronic, optical, and hydrogen storage properties of Li2TiXH6 (X= Cr, Mn) hydrides for an advanced hydrogen storage system, *Int. J. Mod. Phys. B*, 2025, **39**(29n30), 2550261.

29 A. N. Khan, N. U. Khan, M. Kaleem, M. Tanzeel, A. Nasir, A. Hosen, A. Akremi and I. Boukhris, Lead-Free X2MgGeI6 (X= Rb, Cs) Double Perovskites for Multi-functional Energy Applications: A DFT and SCAPS-1D Perspective, *Solid State Sci.*, 2025, 108049.

30 K. El Kihel, Z. El Fatouaki, A. Tahiri, M. Idiri and M. El Bouziani, Electronic structure, Optical, Phonon, Mechanical, Thermodynamic, and Hydrogen Storage properties of A2BH6 (A= Ca, Sr, Ba) perovskite hydrides by DFT calculations, *Phys. B*, 2026, 418219.

31 S. S. Raman, D. Davidson, J.-L. Bobet and O. Srivastava, Investigations on the synthesis, structural and microstructural characterizations of Mg-based K2PtCl6 type (Mg2FeH6) hydrogen storage material prepared by mechanical alloying, *J. Alloys Compd.*, 2002, **333**(1–2), 282–290.

32 S. Al, Mechanical and electronic properties of perovskite hydrides LiCaH 3 and NaCaH 3 for hydrogen storage applications, *Eur. Phys. J. B*, 2021, **94**(9), 182.

33 A. Züttel, P. Wenger, S. Rentsch, P. Sudan, P. Mauron and C. Emmenegger, LiBH4 a new hydrogen storage material, *J. Power Sources*, 2003, **118**(1–2), 1–7.

34 A. Obeidat, A. Alrousan and S. Abu-Rajouh, First-principles study of structural, hydrogen storage, mechanical, electronic, and optical properties of K2NaXH6 (X= Al, As, Bi, Ga, In) double perovskite hydrides, *J. Power Sources*, 2025, **642**, 236944.

35 S. Bahou, H. Labrim, M. Lakhal, M. Bhihi, B. Hartiti and H. Ez-Zahraouy, Magnesium vacancies and hydrogen doping in MgH2 for improving gravimetric capacity and desorption temperature, *Int. J. Hydrogen Energy*, 2021, **46**(2), 2322–2329.

36 A. Hosen, A. A. Mousa, E. Nemati-Kande, A. N. Khan, M. S. Abu-Jafar, E. Benassi, E. Elghmaz, N. Abd EL-Gawaad and J. Asad, Systematic Computational Screening and Design of Double Perovskites Q2LiMH6 (Q= K, Rb; M= Ga, In, Tl) for Efficient Hydrogen Storage: A DFT and AIMD Approach, *Surf. Interfaces*, 2025, 106608.

37 M. Kaleem, M. M. A. Iqbal and A. N. Khan, Stability and hydrogen storage performance of Na 2 LiXH 6 (X= Zr, V, Cr) double perovskite hydrides *via* DFT and AIMD, *RSC Adv.*, 2026, **16**(2), 995–1007.

38 A. Ayyaz, M. Kaleem, A. Nasir, N. D. Alkhaldi, M. mana Al-Anazy, I. Boukhris, Q. Mahmood and M. Z. Abbasi, Investigation of optoelectronic and photovoltaic characteristics of A2NaAlI6 (A= Rb, Cs)-based perovskite solar cells with different charge transport layers: DFT and SCAPS-1D simulation, *Sol. Energy*, 2025, **299**, 113738.

39 R. Song, N. Xu, Y. Chen, S. Chen, J. Zhang, W. Dai and W. Zhang, Insight into the mechanical, electronic, kinetic, thermodynamic, and hydrogen storage properties of XFeH3 (X= Ca, Sr, Ba) perovskites for hydrogen storage applications: first-principle calculations, *Chin. J. Phys.*, 2024, **89**, 1152–1163.

40 B. Rehmat, M. Rafiq, Y. Javed, Z. Irshad, N. Ahmed and S. Mirza, Elastic properties of perovskite-type hydrides LiBeH3 and NaBeH3 for hydrogen storage, *Int. J. Hydrogen Energy*, 2017, **42**(15), 10038–10046.

41 M. Ali, M. Raheel, Z. Bibi, M. A. Rusho, D. Khan, W. Al-Azzawi and R. A. Alshgari, Atomistic simulations for electronic structure, mechanical stability and optical responses of sodium-based NaAH3 (A= Sc, Ti and V) metal hydride perovskites for hydrogen storage applications, *Int. J. Hydrogen Energy*, 2025, **128**, 749–759.

42 X. Yang, Y. Li, Y. Liu, Q. Li, T. Yang and H. Jia, Crystal structure prediction and performance assessment of hydrogen storage materials: Insights from computational materials science, *Energies*, 2024, **17**(14), 3591.

43 A. Es-Smairi, S. Al-Qaisi, N. Sfina, A. Boutramine, H. R. Jappor, H. S. Alzahrani, A. H. Alfaifi, H. Rached, A. S. Verma and M. Archi, DFT insights into the structural, stability, elastic, and optoelectronic characteristics of Na2LiZF6 (Z= Ir and Rh) double perovskites for sustainable energy, *J. Comput. Chem.*, 2025, **46**(8), e70097.

44 S. Takagi, H. Saitoh, N. Endo, R. Sato, T. Ikeshoji, M. Matsuo, K. Miwa, K. Aoki and S.-i. Orimo, Density-functional study of perovskite-type hydride LiNiH 3 and its synthesis: Mechanism for formation of metallic perovskite, *Phys. Rev. B Condens. Matter*, 2013, **87**(12), 125134.

45 F. Qureshi, M. Yusuf, S. Ahmed, M. Haq, A. M. Alraih, T. Hidouri, H. Kamyab, D.-V. N. Vo and H. Ibrahim, Advancements in sorption-based materials for hydrogen storage and utilization: A comprehensive review, *Energy*, 2024, **309**, 132855.

46 Y. Tang, J. Zhang, X. Zhong, Q. Wang, H. Zhang, C. Ren and J. Wang, Revealing the structural, electronic and optical properties of lead-free perovskite derivatives of Rb2SnX6 (X= Cl, Br and I): a theory calculation, *Sol. Energy*, 2019, **190**, 272–277.

47 S. Hayat, R. A. Khalil, M. I. Hussain, A. M. Rana and F. Hussain, First-principles investigations of the structural, optoelectronic, magnetic and thermodynamic properties of hydride perovskites XCuH3 (X= Co, Ni, Zn) for hydrogen storage applications, *Optik*, 2021, **228**, 166187.

48 M. Tanzeel, M. Kaleem, A. N. Khan, A. Nasir, M. Ali, A. Alshamari, A. Ayyaz and A. Almohammedi, A computational investigation of novel double perovskite oxides Ba2XReO6 (X= Li, Na) for optoelectronic and photocatalytic applications, *Int. J. Mod. Phys. B*, 2025, 2650012.

49 A. Ayyaz, M. Kaleem, A. Shakoor, H. D. Alkhaldi, A. Nasir, A. Akremi, H. Albalawi and Q. Mahmood, Investigation of promising stable halide double perovskites K2LiXI6 (X= Al, Ga) for solar cells and thermoelectric device applications: DFT and SCAPS-1D simulation approach, *Chem. Phys. Lett.*, 2025, 142433.

50 H. Murtaza, J. Munir, Q. Ain, A. S. Aldwayyan, H. M. Ghaithan, A. A. A. Ahmed and S. M. Qaid, First-principles prediction of the optoelectronic, mechanical, thermodynamic and hydrogen storage attributes of double perovskite Rb2NaXH6 (X= Al, In) hydrides, *J. Inorg. Organomet. Polym. Mater.*, 2025, **35**(4), 2877–2888.

51 S. Zhang, S. Chen, Y. Chen, J. Hou, D. Xu, W. Luo and Z. Shi, First principles study on the structure, hydrogen storage, and physical properties of X2VH6 (X= Mg, Ca, Sr, Ba) perovskite hydrides for hydrogen storage applications, *Int. J. Hydrogen Energy*, 2025, **166**, 150903.

52 N. Al-Zoubi, A. Almahmoud, A. Almahmoud and A. Obeidat, Theoretical assessment of a novel NaXH3 and KXH3 (X= Tc, Ru and Rh) perovskite hydrides for hydrogen storage, *Int. J. Hydrogen Energy*, 2024, **93**, 822–831.

53 S. Al-Qaisi, N. Iram, N. Sfina, A. Boutramine, H. R. Jappor, A. H. Alfaifi, H. S. Alzahrani, H. Rached, M. A. Ali and G. Murtaza, Comprehensive DFT study of K2TlZI6 (Z= Al, In) double perovskites: Structural stability and potential for optoelectronic and thermoelectric energy harvesting, *Phys. B*, 2025, **710**, 417239.

54 O. L. Anderson, A simplified method for calculating the Debye temperature from elastic constants, *J. Phys. Chem. Solids*, 1963, **24**(7), 909–917.